





## RESEARCH ARTICLE

WILEY

# Connectivity-based parcellation of normal and anatomically distorted human cerebral cortex

Stephane Doyen<sup>1</sup> | Peter Nicholas<sup>1</sup> | Anujan Poologaindran<sup>2,3</sup> |  
 Lewis Crawford<sup>1</sup>  | Isabella M. Young<sup>1</sup>  | Rafeael Romero-Garcia<sup>2</sup>  |  
 Michael E. Sughrue<sup>1</sup> 

<sup>1</sup>Omniscient Neurotechnology, Sydney, New South Wales, Australia

<sup>2</sup>Brain Mapping Unit, Department of Psychiatry, University of Cambridge, Cambridge, UK

<sup>3</sup>The Alan Turing Institute, British Library, London, UK

## Correspondence

Stephane Doyen, Omniscient Neurotechnology Sydney, New South Wales, Australia.

Email: stephane.doyen@o8t.com

## Funding information

Department of Energy, Grant/Award Number: FG02-08ER64581; National Center for Research Resources, Grant/Award Number: U24-RR021992; Center of Biomedical Research Excellence (COBRE), Grant/Award Number: 5P20RR021938/P20GM103472; National Institute of Mental Health, Grant/Award Number: R01MH084898-01A1

## Abstract

For over a century, neuroscientists have been working toward parcellating the human cortex into distinct neurobiological regions. Modern technologies offer many parcellation methods for healthy cortices acquired through magnetic resonance imaging. However, these methods are suboptimal for personalized neurosurgical application given that pathology and resection distort the cerebrum. We sought to overcome this problem by developing a novel connectivity-based parcellation approach that can be applied at the single-subject level. Utilizing normative diffusion data, we first developed a machine-learning (ML) classifier to learn the typical structural connectivity patterns of healthy subjects. Specifically, the Glasser HCP atlas was utilized as a prior to calculate the streamline connectivity between each voxel and each parcel of the atlas. Using the resultant feature vector, we determined the parcel identity of each voxel in neurosurgical patients ( $n = 40$ ) and thereby iteratively adjusted the prior. This approach enabled us to create patient-specific maps independent of brain shape and pathological distortion. The supervised ML classifier re-parcellated an average of 2.65% of cortical voxels across a healthy dataset ( $n = 178$ ) and an average of 5.5% in neurosurgical patients. Our patient dataset consisted of subjects with supratentorial infiltrating gliomas operated on by the senior author who then assessed the validity and practical utility of the re-parcellated diffusion data. We demonstrate a rapid and effective ML parcellation approach to parcellation of the human cortex during anatomical distortion. Our approach overcomes limitations of indiscriminately applying atlas-based registration from healthy subjects by employing a voxel-wise connectivity approach based on individual data.

## KEYWORDS

connectivity, DTI, glioma, machine learning, parcellation, tractography

**Abbreviations:** A-HCP, augmented HCP atlas; COBRE, Centre for Biological Research Excellence; CSD, constrained spherical deconvolution; DART, dropout regularization for regression trees; DES, direct electrical stimulation; DIPY, diffusion imaging in Python; DWI, diffusion weighted imaging; EPI, echo planar imaging; FA, fractional anisotropy; fODF, fiber orientation distribution function; HCP, Human Connectome Project; MCIC, MIND Clinical Imaging Consortium; ML, machine learning; MMP, multimodal parcellation; MNI, Montreal Neurological Institute; MPRAGE, magnetization prepared rapid acquisition gradient echo; MRI, magnetic resonance imaging; SCA, structural connectivity atlas.

This is an open access article under the terms of the Creative Commons Attribution-NonCommercial-NoDerivs License, which permits use and distribution in any medium, provided the original work is properly cited, the use is non-commercial and no modifications or adaptations are made.

© 2021 Omniscient Neurotechnology Pty limited. *Human Brain Mapping* published by Wiley Periodicals LLC.

## 1 | INTRODUCTION

Informative and individual parcellation of the human brain remains an elusive goal in the context of brain deforming pathologies. For over a century, cerebral cartographers have aimed to parcellate the human brain into distinct neurobiologically defined areas (Becker et al., 2020). Early approaches to this problem were dominated by histology-based cytoarchitectonics popularized by Brodmann (2005) and von Economo and Koskinas (1925). In recent decades, rapid advancements in technology and engineering have helped evolve approaches to this age-old problem in neuroscience (Burks et al., 2017). Today, with access to high-resolution multimodal magnetic resonance imaging (MRI) sequences, we can effectively parcellate the healthy cerebral cortex by integrating local properties of brain tissue with long-range connectivity patterns (Dell'acqua & Tournier, 2019). However, the application of these advanced techniques to the deformed brain has been limited.

Recently, Glasser et al. in the Human Connectome Project (HCP) developed a multimodal cortical parcellation scheme by integrating local myelin and cortical thickness features with global task-based and resting-state functional MRI features (Glasser et al., 2016). Moreover, despite the existence of variability between individuals, careful mapping efforts by the HCP revealed remarkable functional and topological similarities between neurologically healthy-normal individuals. The use of big data for parcellating the cerebral cortex has become a defining hallmark of modern brain mapping. Specifically, boundary mapping and clustering/factorization methods to parcellate the healthy human brain have become a gold-standard in the field (Bijsterbosch et al., 2020; Glasser et al., 2016; Glenn et al., 2017). These techniques exploit the intrinsic structure of MRI data to develop data-driven solutions to parcellate the healthy cortex.

Despite this, modern data-driven approaches (i.e., Glasser et al., 2016; Yeo et al., 2011) fail to perform accurately in heavily anatomically distorted clinical cases with small sample sizes, such as brain tumors or strokes (Poologaindran, Lowe, & Sughrue, 2020; Smitha et al., 2017). In these clinical contexts, not only is the underlying anatomy distorted, leading to difficulties in image alignment, processing, and registration methods used in healthy brains (Fan et al., 2016), but the underlying pathology may perturb the MRI signal itself (Glasser et al., 2016). To circumvent this problem, existing methods generally adopt atlas-driven approaches from healthy subjects to parcellate anatomically distorted brains. While such an approach provides a reasonable interim solution to probe the connectome at the group-level, it is not sufficiently accurate for surgical planning at the single-subject level (Burks et al., 2017; Romero-Garcia et al., 2020). Specifically, registration errors, distortion issues, and resolution differences could lead to several millimeters of inaccuracy, limiting the utilization of any template-driven approaches for neurosurgery (Dell'acqua & Tournier, 2019).

To address these limitations, other techniques have been developed including cost-function masking (Brett et al., 2001) and virtual brain-grafting (Radwan et al., 2021). Relative to template-driven

approaches, these techniques offer advantages to parcellating anatomically distorted brains; however, they do not ultimately integrate information about the underlying structural connectivity of the individual patient.

A unifying principle of brain network organization is that the functional relevance of a brain area is dependent on its connectivity with surrounding brain areas (Fischl, 2012; McIntosh, 2004; Pessoa, 2014). None of the parcellation techniques developed thus far take advantage of, and rely on, this unifying principle of structural connectivity and anatomical organization.

Leveraging this principle of anatomical connectivity, we sought to develop a structural connectivity-based “re-parcellation” scheme to the anatomically distorted cerebral cortex. We develop and train a machine learning (ML) classifier that can identify Glasser HCP parcels using easy-to-acquire clinical-grade MRI data, with the aim of producing idiographic parcellations in both healthy and anatomically distorted brains.

## 2 | METHODS

### 2.1 | Normative and patient datasets

#### 2.1.1 | Normal diffusion tractography datasets

The T1-anatomical and diffusion weighted images (DWI) for 178 healthy control subjects were obtained from the Schizconnect (<http://schizconnect.org>) database. The inclusion criteria image collation included subjects with “No Known Disorder” and T1 Magnetization Prepared Rapid Acquisition Gradient Echo (MPRAGE) and Structural Diffusion MRI scans acquired on a 3 T scanner. This query yielded 178 unique subjects with the requisite data. Ninety-four subjects were from the MIND Clinical Imaging Consortium (MCICShare) and 84 subjects were from the Centre for Biological Research Excellence (COBRE). For the T1 MPRAGE in the MCICShare dataset, the voxel size was  $0.703 \times 1.5 \times 0.703$  mm, and the image dimensions were  $256 \times 144 \times 256$  mm. For the DWI in the MCICShare dataset, the voxel size was  $2 \times 2 \times 2$  mm, the image dimensions were  $128 \times 128 \times 60$  mm and the DWI sequence consisted of 60 non-collinear diffusion weighted gradient directions ( $b = 700$  s/mm) and 10 additional images without diffusion weighting ( $b = 0$  s/mm). For the T1 MPRAGE in the COBRE dataset, the voxel size was  $1 \times 1 \times 1$  mm, and the image dimensions were  $192 \times 256 \times 256$  mm. For the DWI in the COBRE dataset, the voxel size was  $2 \times 2 \times 2$  mm, the image dimensions were  $128 \times 128 \times 72$  mm and the DWI sequence consisted of 34 noncollinear diffusion weighted gradient directions ( $b = 800$  s/mm) and one additional image without diffusion weighting ( $b = 0$  s/mm). A complete list of acquisition parameters can be found “Imaging Data Information” at: <http://schizconnect.org/documentation>. As a result, the heterogeneity of voxel resolution and size constituted an excellent test of generalizability of our algorithm.

### 2.1.2 | Hold out sample

To confirm that our approach would generalize well to other scan data acquisition protocols (e.g., different scanner), we tested our structural connectivity-based brain atlas (SCA) on an out-of-cohort dataset of 52 healthy control brains from the University of California Los Angeles (UCLA) Consortium for Neuropsychiatric Phenomics LA5c Study Dataset provided by OpenNeuro (<https://openfmri.org/dataset/ds000030/>; accession number ds000030). The dataset consisted of 52 subjects with a T1 MPRAGE and Diffusion Data MRI Protocols on 3 T scanners. The T1 MPRAGE data had voxel size  $1 \times 1 \times 1$  mm with image dimensions of  $176 \times 256 \times 256$  mm. The DWI data has voxel size of  $1.979 \times 1.979 \times 2$  mm, image dimensions of  $96 \times 96 \times 60$  mm and the DWI Sequence consisted of 64 non-collinear diffusion weighted gradient directions ( $b = 1,000$  s/mm) and one additional image without diffusion weighting ( $b = 0$  s/mm).

### 2.1.3 | Brain tumor patient sample

To study the performance of our model in brain tumor patients, we randomly selected 40 cases of patients with World Health Organization (WHO) grade 2–4 supratentorial infiltrating gliomas from a surgical imaging dataset operated on by the senior author between 2012 and 2018. These images were collected for purposes of surgical planning and studied with approval of the patient and the institutional review board (IRB #3199). The collected scans included an anatomical T1-weighted image and DWI series. Diffusion imaging was performed on a 1.5 T GE Optima with the follow settings: Spin-echo echo-planar imaging (EPI) DWI, with 24 diffusion weighted directions ( $b = 1,000$  s/mm) and one additional image without diffusion weighting ( $b = 0$  s/mm), field of view (FOV) = 25.6 cm, slice thickness 2.5 mm, 0 mm gap between slices with no overlap, full brain coverage, voxel size  $1.016 \times 1.016 \times 2.5$  mm, square  $256 \times 256$  matrix, 1 average/number of averages (NEX), and axial foot to head slice prescription.

### 2.1.4 | HCP test–retest data

The T1-anatomical and diffusion weighted images for 44 healthy control subjects were obtained from the Human Connectome Project. The HCP test–retest dataset is a subset of the overall 1,200 MRIs. Forty-five subjects received a secondary scan between 1 and 11 months after their initial scan. One subject did not have diffusion data available for tractography and so was excluded from the study. The anatomical images are T1 axial images with a FOV of  $224 \times 224$  mm, voxel size 0.7 mm isotropic. The DWI images consisted of five images without diffusion weighting ( $b = 0$  s/mm) and 90 gradient directions with 30 noncollinear directions each at  $b = 1,000$ ,  $b = 2,000$ , and  $b = 3,000$  s/mm. The DWI image dimensions were  $144 \times 168 \times 111$ . The test–retest data was used to confirm the stability and consistency of the SCA on a single subject at

different time points. The degree of biological change over this period is expected to be small.

## 2.2 | Diffusion weighted images pre-processing

DWI images were processed using the prescribed processing steps from the diffusion imaging in Python (DIPY) package available in the Python language including correcting for motion, extraction of the brain, and correction for gradient distortion (Garyfallidis et al., 2014). Specifically, DWI images were motion corrected by aligning each time frame to the initial b0 image using translation and rigid body registration (Leemans & Jones, 2009). Brain extraction on the DWI was performed using the Otsu thresholding technique. The anatomical image was skull stripped using the HD-BET (Division of Medical Image Computing at the German Cancer Research Center (DKFZ) (<https://github.com/MIC-DKFZ/HD-BET>; Isensee et al., 2019). The skull stripped anatomical image was registered against the DWI image via a successive translation registration and rigid body registration. Correction for gradient distortion was achieved by allowing the DWI to diffeomorphically warp against the registered anatomical image.

The resulting images were then resliced into  $2 \times 2 \times 2$  mm isotropic voxels. The fiber orientation distribution function was calculated using the constrained spherical deconvolution (CSD) (Tournier, Calamante, Gadian, & Connelly, 2004) tool provided in DIPY (Garyfallidis et al., 2014). The fiber orientation distribution function (fODF) was calculated with CSD with a spherical harmonic order of 6. CSD peaks were extracted from the model using a relative peak threshold of 0.5 and a minimum separation angle of  $20^\circ$ . Using the EuDX algorithm which uses Euler integration and trilinear interpolation in conjunction with a set of stopping criteria (Garyfallidis, Brett, Correia, Williams, & Nimmo-Smith, 2012). Deterministic tractography was then performed with four fibers per voxel seeded evenly throughout white matter voxels as determined by a fractional anisotropy (FA) value of above 0.3 (Auriat, Borich, Snow, Wadden, & Boyd, 2015; Cheng et al., 2012).

## 2.3 | Model and performance metrics

### 2.3.1 | Generation of a cortical and subcortical atlas

We began with the Human Connectome Project Multi-Modal Parcellation version 1.0 (HCP\_MMP1) with 180 cortical areas in each hemisphere. We added 19 subcortical areas from the FreeSurfer average atlas “RB\_all\_2008-03-26.gca” (Fischl, 2012). These subcortical areas were the left and right cerebellum, thalamus, caudate, putamen, pallidum, hippocampus, amygdala, accumbens, ventralDC, and brainstem as defined in the atlas. These two atlases were combined by acquiring the files in MNI standard space and taking the union of the two atlas schemes. Given that there is no overlap across the two atlases, the end result is a combined cortical and subcortical atlas, hereby referred to as the augmented HCP (A-HCP) atlas.

### 2.3.2 | Creation of a structural connectivity-based brain atlas

We next trained a ML model to recreate the A-HCP atlas based on diffusion weighted structural connectivity (Glasser et al., 2016). Figure 1 provides a schematic of the conceptual basis behind this step, which we call “re-parcellation.” This novel method was created by training the model using the data from healthy subjects in the datasets described previously.

The tractography data was used in conjunction with the initial parcellation fit to create a structural connectivity representation of the data. The A-HCP atlas in MNI space was then warped onto each brain. Tract endpoints from the CSD tractography were then used to generate a voxel to parcel structural connectivity vector. For each voxel, we parsed the CSD tractography and identified streamlines that started or terminated in that voxel. Then the endpoints of these streamlines were used to build a feature vector on the number of streamline connections between that voxel and each of the 379 parcels in the A-HCP atlas. Calculating this over all voxels generated a voxel to parcel structural connectivity matrix.

The voxel-to-parcel feature vector (structural connectivity) matrix had 379 dimensions corresponding to the 379 parcels included in the A-HCP atlas. All dimensions were used in classification; and no feature selection was used before classification. This feature vector could then be used for training and classification. Figure 2 provides a schematic description of the process used to generate voxel-to-parcel feature vectors.

The voxel-to-parcel feature vectors for each parcel in the structural connectivity matrix were then used as a training set to fit a gradient boosted tree-based model (XGBoost). To ensure clinical relevance of the model we optimized the algorithm on precision. This leads to a supervised learning paradigm in which voxel to parcel structural connections are used to train and predict each parcels category. This trained model can then be applied to classify voxels in subsequent subjects' brains. In application, the voxel-wise structural connectivity feature vector is constructed as before and used to determine the parcel identity of each voxel. This creates a voxel-wise recreation of the A-HCP atlas with subcortical components, which is independent to brain shape and pathologic distortion while being subject-specific yet comparable between subjects. Additionally, classification is constrained around the centroid of the target parcel, which is utilized to constrain the voxels studied for assignment of a given parcel to a plausible area in the vicinity of its typical position. Only voxels with streamline fibers starting or terminating in them are classified. In cases of a structural lesion, white matter no longer exists. Accordingly, no tractography is traced to these voxels and the model does not classify any parcels. Given the dependence on white matter endpoints to reach a classification for that voxel, we acknowledge that structural connectivity-based classification we have proposed will not be able to fully recreate the voxel coverage of the warped A-HCP. However, by providing an accurate prediction over a subset of the gray matter voxels, this model can still be useful for clinical purposes where

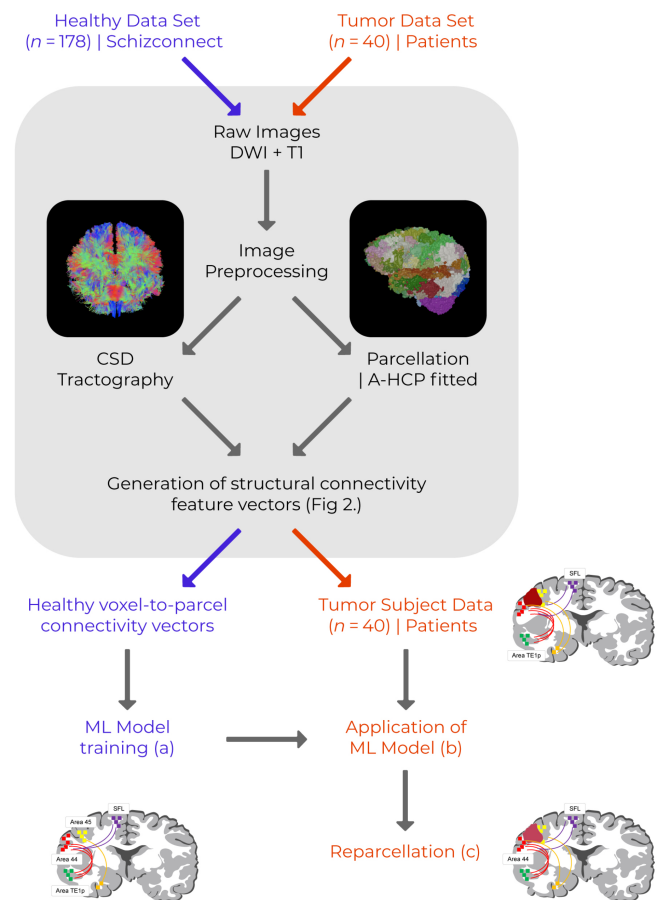


**FIGURE 1** Schematic description of the structural connectivity atlas (SCA) re-parcellation pipeline. (a) The SCA machine-learning model is first trained by entering preprocessed tractography data from healthy subjects to learn the structural connectivity patterns between voxels included within the 379 parcels identified by our augmented version of the HCP\_MMP1 (A-HCP) atlas (Schizconnect data set,  $n = 178$ ). (b) Physically distorted tractography data is then preprocessed identically to the healthy cohort, and structural connectivity patterns are calculated for each cortical voxel (Tumor patient data set,  $n = 40$ ). (c) The machine-learning model is then applied to each individual in the patient data set, and voxels located at tract endpoints are appointed their most likely A-HCP parcellation based on their structural connectivity feature vectors, resulting in the re-parcellation of voxels where physical distortion has shifted the mapping of the A-HCP atlas

clinicians only need to see a sparse amount of voxel predictions to have an informed insight into that region of the brain.

### 2.3.3 | Machine learning model framework

The statistical model used is a gradient-boosted decision tree model (XGBoost) (Chen & Guestrin, 2016). This classifier uses ensembles of decision trees to build a statistical map between the voxel level feature vector and the most probable parcellation class, where

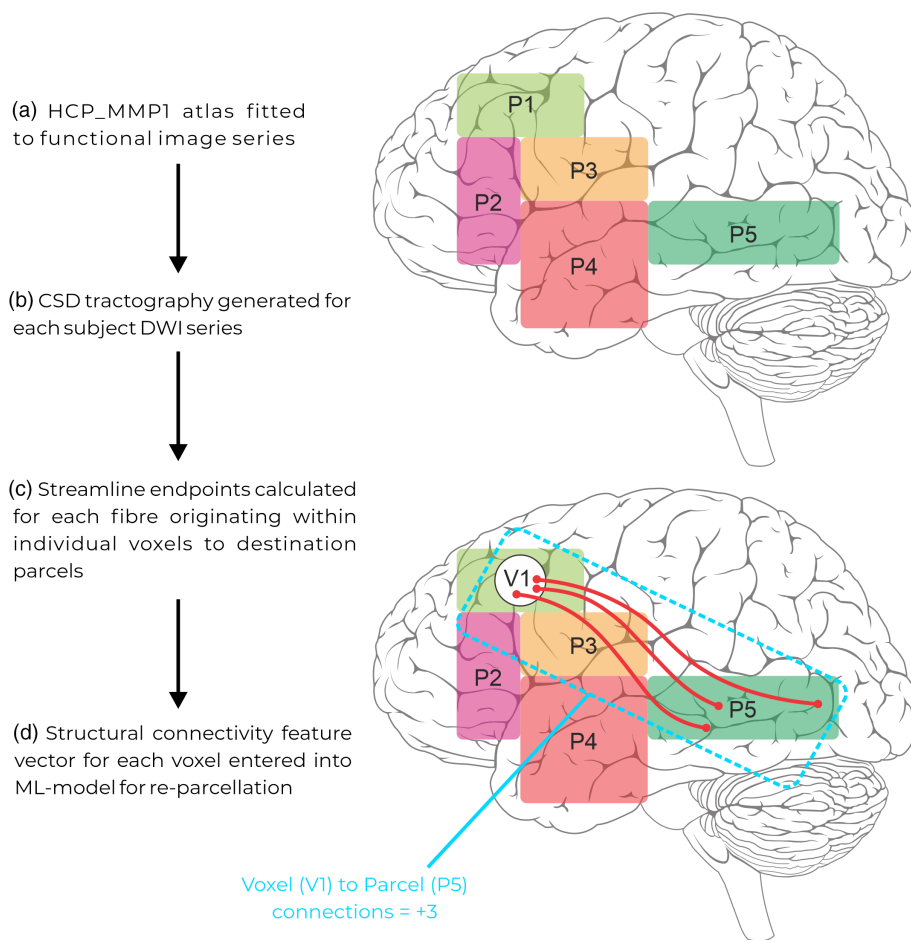


**FIGURE 2** Generation of voxel-to-parcel feature vectors. (a) The augmented HCP\_MMP1 atlas is fitted to a functional image series, defining the boundaries and voxels included in each of the 379 A-HCP parcels. (b) Diffusion weighted image (DWI) series undergo constrained spherical deconvolution (CSD) to map the course of white matter tracts within the cortex. (c) Individual streamlines originating within each voxel are derived, and their endpoints mapped to all other cortical parcels. (d) The number of streamlines ending in each parcel are counted and entered as a structural connectivity feature vector for each individual voxel of each parcel. In this example, a voxel in parcel A (V1; white) has three streamline endpoints terminating within parcel E (P5; dark green), which is entered as the feature vector for this voxel

“parcellation class” refers to any single brain region included in the A-HCP atlas. Gradient boosted decision-trees have several advantages over generic decision trees in flexibility and the ability to incorporate varied feature sets. XGBoost in particular has several performance enhancements over other implementations of gradient-boosted decision trees, namely in the speed and memory improvements that parallelization and memory management bring, as well as the dropout regularization for regression trees (DART) to reduce the potential of overfitting. In the case of the SCA, maximizing precision is favorable as it reflects the ability to recreate the A-HCP atlas from the structural connectivity data.

### 2.3.4 | Model similarity assessment

To determine the ability of our model to appropriately identify the 379 cortical and subcortical areas in normal brains, we utilized the registered A-HCP atlas as a “ground truth.” We tested the proportion of concordance between voxels from the co-registered A-HCP and the SCA for held out, out of sample subjects. Because of the dependence on white matter endpoints to reach a voxel prediction, we do not expect the model to completely regenerate the registered A-HCP atlas. However, for the subset of voxels that receive a classification

by the SCA, they should largely be consistent with the registered A-HCP. Additionally, the stability of the model was assessed by repeating the generation of the SCA twice across 30 normal brains from the held out, out of sample subjects. Differences between successive runs were analyzed to determine how much, if any, deviation occurred between runs on each subject.

### 2.3.5 | Assessment of our pipeline steps and machine learning parcellation in tumor patients

To determine if the ML generated re-parcellation scheme was plausible, we validated our model using the following criteria: (a) parcels involved no assigned voxels in a resected cavity or region of necrotic tumor, (b) parcels reassigned due to tumor presence are pushed in a direction concordant with the tumor mass effect, (c) parcels are on the correct side of subarachnoid landmarks, such as the Sylvian fissure, and (d) white matter structures appear to support the parcels identified as noted in tractographic descriptions of the Cerebrum (Briggs et al., 2018; Briggs et al., 2018a, 2018b; Sali et al., 2018; von Economo & Koskinas, 1925).

In addition, we sought to statistically evaluate the difference between the template-based registration of A-HCP-MMP1.0

(volumetric) Glasser atlas and our subject-specific SCA methodology. Specifically, we calculated the overall accuracy between the SCA and the registered atlas over a dataset of tumored/resected brains under two conditions. First, we calculated the accuracy between the two atlases over voxels that both systems assigned to a parcel. Second, we calculated the accuracy between the two atlases over all voxels that the template atlas assigned to a parcel. We would expect the difference between these two measures of accuracy to be much larger than in the hold out sample. This is because the SCA only predicts voxels with white matter endpoints and because these endpoints would not exist in areas of tumor or resection. Conversely the registration approach (standard application of the A-HCP atlas) would falsely assign parcels to these areas.

### 3 | RESULTS

Overall, the SCA generated plausible imaging results for all 40 tumor subjects we investigated in accordance with our set of visual assessment criteria. We then further investigated the integrity of the machine-learning model by calculating model metrics against the fitted A-HCP atlas as a “ground truth” to quantitatively assess its performance.

#### 3.1 | Precision performance of the SCA

We tested the overall performance of the model by calculating the recall and precision of the SCA versus the co-registered A-HCP atlas-based approach. Importantly, as the SCA model necessitates tract terminations in the voxel of interest to build the required feature vector, thereby only mapping voxels which contain the required streamline endpoints. Thus, the overall cortical coverage of the SCA is much lower than the A-HCP. This property supports the clinical value of the SCA as it aims not to fully classify every gray matter voxel but rather provide classification over a subset of voxels that are precise in cases of resection and tumor. In a clinical setting, providing accurate classification over a sparse subset of voxels is sufficient in giving clinicians an informed view of where key parcels are located within the brain.

Precision is a measure of the number of predictions of the positive class that actually belong to the positive class. It is calculated as the number of true positives as a proportion of the sum of true positives and false positives. Recall is a measure of the number of positive class predictions out of all positive classes. It is calculated as the number of true positives as a proportion of the sum of true positives and false negatives. F1 score (or F score) is the weighted average of precision and recall and takes into account both false positives and false negatives. As Table 1 shows, the average classifier recall was 97.1% and the average precision was 98.0% when compared with the A-HCP atlas as ground truth. The average classifier accuracy was 96.2% and the average F1 score was 97.6% when compared with the A-HCP atlas as ground truth.

Further, to test for parcel-specific performance we tested each of the 379 parcels separately using a bounding box extending ~2 cm beyond the boundaries of the parcels as provided by the registered A-HCP atlas. Overall, and in keeping with the clinical preference for an optimization towards precision, most parcels showed a high degree of precision and comparatively lower recall. The distribution of precision, recall, accuracy, and F1 scores are displayed in Figure 3.

#### 3.2 | SCA run time

The run time of the SCA from initial brain scans to parcellation was calculated across the hold-out dataset. The run times varied from 37 to 45 min with a mean of 41 min and a SD of 2.5 min. Run times were measured on a 4 CPU, 16 GB RAM m5.xlarge cloud computing instance provided by Amazon EC2. Variation here is primarily due to the number of streamlines generated at the tractography stage. In cases where more streamlines were generated the voxel to streamline connectivity feature vectors took longer to generate and the overall SCA took longer to complete.

Overall, the SCA run time includes image preprocessing and tractography generation. If more streamlines are used, then this increases the amount of time it takes to iterate through all streamlines and create a structural connectivity feature vector. However, the time it takes to use this vector for prediction is constant, as is the time it takes to recreate the atlas.

#### 3.3 | The SCA produces plausible re-parcellation results

Re-parcellation is defined as those voxels which are classified by the SCA approach as having a different parcel than that which was assigned by the fitted A-HCP atlas. In the healthy hold out sample, an average of 2.65% of the classified voxels were identified as being re-parcellated, or on average 662 voxels per subject. In order to increase the understanding of this result, we sought to investigate whether these were clear errors in classification or whether they are plausible instances.

**TABLE 1** Recall and precision results of the SCA when compared with either co-registered A-HCP as ground truth or a one versus all bounding box around each voxel

Metric	Recall/precision value (%)
Average recall (nonoverlapping bounding box)	96.8
Average precision (nonoverlapping bounding box)	96.9
Average recall (vs. A-HCP ground truth)	97.1
Average precision (vs. A-HCP ground truth)	98.0
Average accuracy (vs. A-HCP ground truth)	96.2
Average F1 (vs. A-HCP ground truth)	97.6

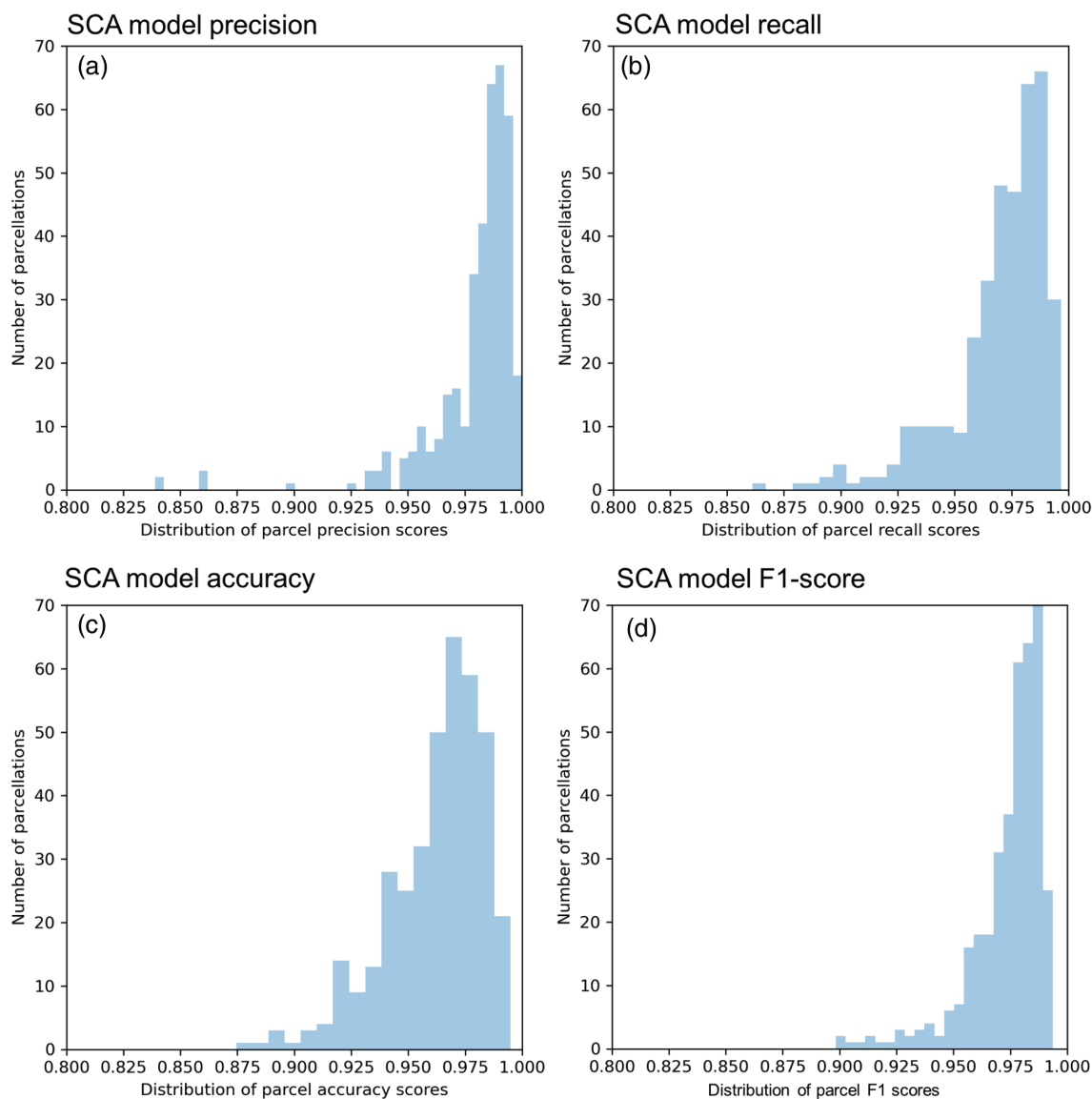


**FIGURE 3** SCA precision and recall performance on out-of-cohort data set. (a) Distribution of precision scores for each parcellation included in the SCA—higher precision scores indicate a greater confidence of predicting parcel identity when anomalous brain scans are entered into the machine learning model. (b) Distribution of recall scores for each parcellation included in the SCA—a higher recall score indicates that for a given parcel, a larger number of potential voxel predictions were accurately made. Thus recall provides insight into the ability of the model to find parcel voxels. (c) Accuracy scores for each parcellation in the SCA atlas—accuracy is the proportion of correct predictions to total predictions. (d) F1 score (or F score) for each parcellation in the SCA atlas—F1 score represents weighted average of precision and recall and takes into account both false positives and false negatives

### 3.3.1 | Re-parcellation primarily occurs to adjacent neighbor parcels

For each of the re-parcellated voxels, we assessed whether or not that voxel was changed to a parcel that was an adjacent neighbor from the fitted atlas designated parcel. Adjacent neighbor parcels are defined as those that are spatially connected by a voxel surface in 3D space. In this approach, we can view voxel identity re-attribution to adjacent parcels as plausible, while re-attribution to distant or nonadjacent parcels as implausible. Seventy-six percent of the re-parcellated voxels were found to have been changed to a parcel that was an adjacent

neighbor to the fitted atlas designated parcel. This indicates that while the SCA is only slightly different from the fitted atlas in healthy subjects, the deviations themselves are highly biologically plausible.

Moreover, the consistency of the SCA or the stability of results between successive runs, was measured by generating the SCA for the 44 test-retest subjects from the HCP dataset. Across each of these subjects, the SCA generated across successive runs was largely consistent. The accuracy between the test and retest generated SCAs was 79%. By accuracy we refer to the number of voxels that are given the same parcel classification between test and retest, as a proportion of the number of voxels that receive a classification in both test and

retest data. This was expected given the stability in tractography seeding and the deterministic quality of the ML algorithm. Notably, some degree of variation is expected given the variances inherent in CSD tractography.

### 3.3.2 | The SCA demonstrates plausible re-parcellation in abnormal brains

To test the clinical relevance of the approach, the SCA was applied to 40 patients with known brain abnormalities such as tumors. Results were visually inspected to ensure that no voxels were assigned in a cavity or necrotic tumor and that re-parcellations pushed the atlas towards a structure that was plausible given the mass effect for the tumor. Figure 4 demonstrates example cases of re-parcellation within abnormal brains by utilizing the SCA.

We next compared model metrics of the template-based registration of the A-HCP to the SCA in abnormal brains. The accuracy between these two parcellations schemes was 94% in voxels covered by both approaches. This is slightly less than the accuracy of ~97% that was achieved on normal brains from the out-of-cohort dataset, and shows that the incidence of re-parcellation increases from 2.65% on healthy brains to approximately 5.5% on abnormal brains. Taken together, these scores suggest that the SCA suitably recreated the parcellation schema of the A-HCP in a subject specific manner. We hypothesized greater re-parcellation would occur in physically abnormal brains generally, and an accuracy score of 100% in healthy controls would reflect a complete overlap between the two approaches, that no re-parcellation had occurred, and null the need for the SCA approach. A further corollary is that the registration approach effectively leads to cortical voxels being assigned to areas of resection or tumor. This demonstrates the limitations of the registration approach and elucidates the needs for taking into consideration structural connectivity.

## 4 | DISCUSSION

Parcellation of the anatomically distorted cerebral cortex is of core importance to neurosurgery and the better translation of connectomic techniques into surgical care. For the first time, this study provides a connectivity-based supervised ML approach to parcellate anatomically distorted cerebral cortices. While previous methodologies typically require structurally intact brains to parcellate the brain (Becker et al., 2020; Bonney et al., 2017; Panesar et al., 2019), we demonstrate that a voxel-wise ML classifier is able to distinctly parcellate the cortices of patients with brain tumors and previous cortical surgeries. Importantly, advancing on existing clinical and scientific approaches, the present work enables improved within-patient and cross-patient comparisons despite altered anatomy.

Structural connectivity based parcellations have shown remarkable success in generating robust and anatomically consistent parcellations of the human brain. These methodologies are generally

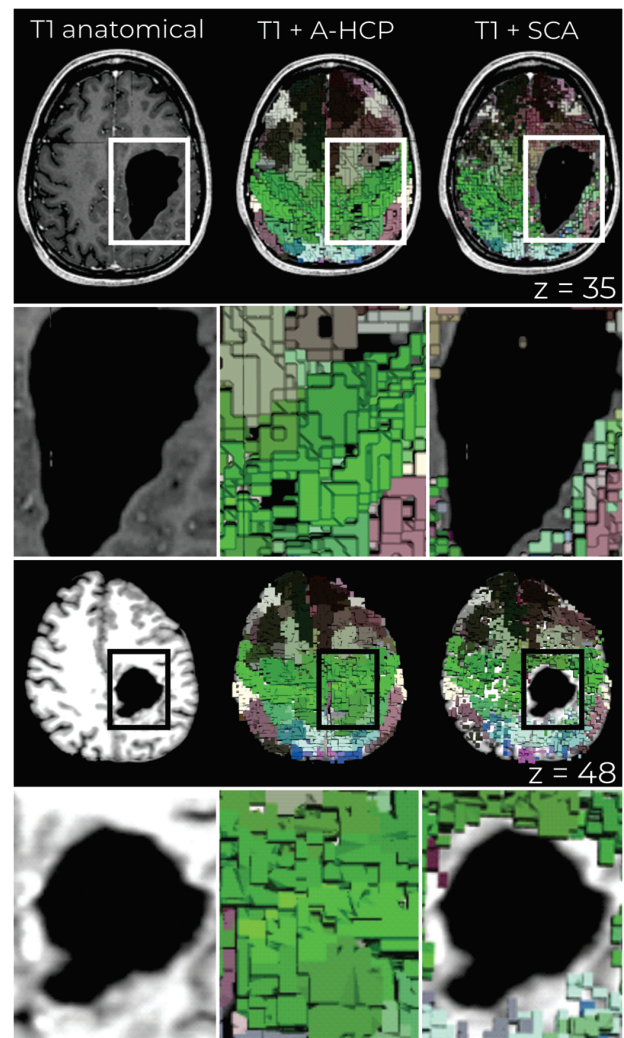


**FIGURE 4** Exemplar pathological tumor sites re-parcellated through the SCA. Color images demonstrating examples of re-parcellation in subjects with tumors following resection. Left column: standard T1-weighted image showing tumor site. Middle column: T1-weighted image overlaid with the augmented HCP (A-HCP) atlas. Right column: T1-weighted image overlaid with the SCA. Top row: right-sided tumor resected from the junction of the parietal and temporal lobes. Bottom row: right-sided parietal lobe tumor resection. In line with our visual validation metrics, these three examples demonstrate that: (1) parcels involved no assigned voxels in resected cavities (however, due to the slice angle displayed, voxels on the tumor boundaries may appear to overlie resected cavities), (2) reassigned parcels were pushed in directions concordant with the mass effect of the tumor site, (3) parcels were assigned on the correct side of anatomical landmarks—such as the falx cerebri in the middle rows, and finally, (4) that parcel structures support those identified in previously published descriptions of the human cerebrum

built around constructing a voxel-wise connectivity profile of the brain with diffusion data. Notably, the Brainnetome project leverages local structural connectivity to parcellate the brain into subregions that are different from each other but internally homogeneous (Fan et al., 2016). The automatic tractography-based parcellation pipeline (ATPP) provides an open-source workflow for tractography-based



parcellation to cluster and label voxels with similar connectivity profiles based on streamline connections to the rest of the brain (Li et al., 2017). Wang et al. (2016) identified that using voxel-wise structural connectivity profiles to generate a connectivity-based atlas produced consistent patterns across subjects and led to a re-configuration from the AAL-90 atlas used as a comparison. Additionally, Honnorat, Parker, Tunç, Davatzikos, and Verma (2017) tested a framework for using structural connectivity to adjust and re-parcellate an anatomical atlas prior demonstrating that it could be used to improve coherence within a parcel. While the SCA is distinct in its focus on accurate re-parcellation of anatomically distorted human cortices, existing methodologies in healthy individuals have demonstrated the advantageous use of structural connectivity for brain parcellation. While the structural connectome constrains functional communication dynamics, additional studies incorporating multimodal data (i.e., resting-state and/or task-based fMRI) are needed to determine if further re-parcellation improvements are possible.

#### 4.1 | Clinical advantages of re-parcellating scheme

A central goal in neurosurgery is to have a firm set of guidelines on brain regions to avoid resecting to prevent neurological decline (Becker et al., 2020; Glenn et al., 2017; Panesar et al., 2019). While some structure–function relationships are firmly established, for example that damage to the corticospinal tract causes long-term contralateral motor deficits, in most cases it is difficult to avoid postoperative cognitive deficits. Thus, with improved brain mapping strategies for the distorted connectome, we are poised to re-formulate the tenets of cortical neurosurgery with additional connectomic data (Rijnen et al., 2019). We believe this process of determining what not to do in surgery is hindered by the difficulty of being certain about what regions were truly removed during surgery.

Structural connectivity provides a topologically invariant method to describe network dynamics (Jin, Zheng, Liu, Guo, & Sun, 2018); thus, we sought to use this as a basis for assigning a voxel to a parcel. Simply put, even when the brain's gross anatomy is altered after surgery, a brain region should not change what it is connected to. Some limitations on this statement need to be made, namely, that it is unlikely that the same image processed using diffusion tractography would produce exactly the same set of connections, so we would not expect preoperative and postoperative imaging to be directly comparable. However, it is likely that the inability to identify a parcel in this method, which would be caused by a significant reduction in the number of voxels in a parcel, implies that all or some of this parcel was resected. Verifying this hypothesis and determining its clinical and neuropsychological ramifications is an area that is being actively studied.

In research and unconstrained scientific environments, MRI acquisition protocols and sequences can provide unprecedented detail into the living human brain. However, in fast-paced clinical environments, technical expertise and scan time make it impractical to routinely use research-grade scan protocols. With regards to our proposed work,

while CSD-based diffusion reconstruction is optimized for higher  $b$ -values, we must balance the demands of a busy clinical workflow and reasonable acquisition parameters. Recently, Toselli et al. (2017) demonstrated that CSD-based estimation of the ODF is possible with clinically achievable lower  $b$ -values with satisfactory performance. Moreover, Calamuneri et al. (2018) also demonstrate that CSD outperforms DTI even in low-hardware settings to investigate white matter integrity. Thus, deploying the proposed re-parcellation scheme with a clinical MRI scan further improves the likelihood of clinical adoption of this technology.

#### 4.2 | Atlas-based parcellation versus connectivity-based re-parcellation

The more traditional methods of matching cortical anatomy to parcel identity include matching to a volume-based atlas, which is well known to have inaccuracies given the differences in folding patterns, and surface based parcellation-schema, such as performed by the widely used software package Freesurfer (Fischl, 2012). While it is an elegant solution to the problem of parcellating the cortical surface despite variable folding patterns, Freesurfer is critically challenged when trying to apply it to the patients with abnormal brains. Furthermore, Freesurfer utilizes a set of surface polygons to tessellate the cortical surface to define anatomic vertices. During the “fix topology” stage of this pipeline, these polygons are adjusted to create a surface with the Euler number of a sphere. However, patients who have had intra-axial surgery have a cortical disruption and thus do not always have a cortex with spherical topology. Moreover, Freesurfer struggles significantly trying to parcellate the brains of tumor patients, even assuming that there has been no cortical reorganization. Our connectivity-based re-parcellation method makes no such assumptions about shape or cortical topology and uses connectivity data to define gray matter structures and parcel location. Thus, its unique versatility enables it to be more clinically realistic and robust to complex patients.

Image pre-processing for diffusion weighted images with some of the most popular platforms, such as Freesurfer, often take several hours. While this has quickened recently by FastSurfer, it remains unclear whether it could handle abnormally shaped brains as the convolutional neural net is trained on the aparc model created by the FreeSurfer pipeline (Henschel et al., 2020). Our model has obvious advantages for clinical neuro-oncology practice, where the data is required quickly, due to some patients needing immediate surgery. FastSurfer still utilizes many of the FreeSurfer pipelines, and despite being faster, given the numerous other steps other than their convolutional neural net, is still time-consuming (Henschel et al., 2020). The SCA processing pipeline takes less than 1 hr to run to completion, benefitting both clinical settings where patients require fast and accurate imaging analysis, particularly in cases of brain tumors, and in research settings, such that data could be collected and analyzed more efficiently.

Notably, atlas-based approaches fail when applied to patients with structurally abnormal brains such as stroke, hydrocephalus,

traumatic brain injury, and atrophy. This is typically due to displacement of the gyri and sulci that these methods attempt to structurally map (Desikan et al., 2006). It is common in these cases for parcels, specific functional areas, and their connections, to be missing due to the tumor or surgical intervention. Additionally, the possibility that functional areas have been reorganized due to the disease process cannot be investigated by these atlas-driven approaches.

### 4.3 | Practical advantages of this approach

To impact and improve clinical care, neuroimaging processing and analysis requires a fast and automated approach that is able to handle pathologic brain anatomy in a robust and biologically accurate way (Briggs et al., 2021). The key benefit of this approach is that it is fast, does not require human input, and in our experience does not crash or struggle with abnormal brains. Methods which cannot accomplish processing in a clinically realistic timeline and without expert input, will not scale to the greater clinical neuroscience community, and in our opinion, does not seem to be a direction worth building towards, if the goal of our research is to provide better diagnostic methods for patients.

### 4.4 | Study limitations

Despite the methodological advances of re-parcellating the cortex using voxel-wise structural connectivity, it is crucial to note that function cannot be attributed to these new parcels in anatomically distorted brains. For example, while area L\_44 (a portion of the canonical Broca's area) is re-parcellated based on connectivity, it is unclear whether it is performing the exact same function as the parcel in anatomically intact brains. This neuroscientific question deserves further attention and is of broad clinical significance. Furthermore, given the inherent limitations of DWI, ground-truth is difficult to discern, not only in healthy subjects, but especially in glioma patients (Ille et al., 2019). For example, the function and purpose of remnant white matter in some developing tumors requires further analyses. However, future studies can harness unique strategies from neurosurgery (i.e., direct intraoperative stimulation) to validate such limitations. Finally, little is known about how cortical reorganization occurs in these patients and what intraoperative and/or clinical phenotypes result from manipulation or loss of a region. Consequently, certainty over the accuracy of a remapped parcel can only be achieved by within-subject and between-subject comparisons.

### 4.5 | Future directions

Ultimately, our study represents a first step toward parcellating anatomically distorted brains in neurosurgical patients. Future directions should involve: (a) testing the utility of multimodal imaging data, (b) increasing the normative and patient sample sizes in which the

model is developed and tested on, and (c) validating the tractography with intraoperative direct electrical stimulation (DES) and behavioral testing. First, the Glasser HCP atlas was derived from high-resolution multimodal anatomical and functional imaging data, which could be acquired in neurosurgical patients. While attractive and possible in research settings, the cost–benefit ratio would need to be evaluated if an improved model (due to multimodal data and increased scan time) is practical in low-resource and fast-paced clinical environments. Second, the use of increased healthy subject data from large imaging consortia may aid in the initial training stage of our model. Moreover, multicentric and open-source international imaging collaborations will enable the improvement of the presented model through harnessing more patients and subsequent imaging data. Finally, prospectively evaluating the ground truth of the re-parcellation scheme with intraoperative DES and behavioral testing would provide additional data to evaluate the performance of our model. This could be readily tested in patients who have already undergone surgery with existing diffusion data and intraoperative testing performed.

## 5 | CONCLUSION

We demonstrate a rapid and efficient method for generating a ML approach to utilize structural connectivity to create a parcellation, allowing us to define anatomy in structurally abnormal brains. While further work will be needed to validate the accuracy of these mapped regions, this proof of concept raises the exciting idea that structurally complex brains, such as those seen in brain tumor patients, can be studied in a clinically applicable setting and workflow, meaning that clinical translation of connectomics is possible in a much broader and pathological patient population than previously studied in the field.

### ACKNOWLEDGMENTS

Data was downloaded from the following sources:

- The Collaborative Informatics and Neuroimaging Suite Data Exchange tool (COINS; <http://coins.mrn.org/dx>) and data collection was funded by National Institute of Mental Health R01MH084898-01A1
- The Collaborative Informatics and Neuroimaging Suite Data Exchange tool (COINS; <http://coins.mrn.org/dx>) and data collection was performed at the Mind Research Network, and funded by a Center of Biomedical Research Excellence (COBRE) grant 5P2ORR021938/P20GM103472 from the NIH to Dr. Vince Calhoun.
- The Neuromorphometry by Computer Algorithm Chicago (NMorphCH) dataset (<http://nunda.northwestern.edu/nunda/data/projects/NMorphCH>)
- The Function BIRN Data Repository (<http://fbirnbd.birncommunity.org:8080/BDR/>), supported by grants to the Function BIRN (U24-RR021992) Testbed funded by the National Center for Research Resources at the National Institutes of Health, USA.

- The Mind Clinical Imaging Consortium database through the Mind Research Network ([www.mrn.org](http://www.mrn.org)). The MCIC project was supported by the Department of Energy under Award Number DE-FG02-08ER64581. MCIC is the result of efforts of co-investigators from University of Iowa, University of Minnesota, University of New Mexico, Massachusetts General Hospital.

## CONFLICT OF INTEREST

Peter Nicholas, Lewis Crawford, Isabella Young, Stephane Doyen, and Michael Sughrue are employees of Omniscient Neurotechnology, who own the intellectual property of the discussed code. Anujan Poologaindran and Rafeael Romero-Garcia do not report any conflict of interest.

## AUTHOR CONTRIBUTIONS

**Stephane Doyen:** Conceptualization, Methodology, Software, Analysis, Supervision. **Peter Nicholas:** Software, Writing - Original Draft, Investigation, Data Curation, Analysis. **Anujan Poologaindran:** Writing - Review & Editing, Interpretation. **Lewis Crawford:** Writing - Original Draft, Validation. **Isabella M. Young:** Writing - Review & Editing, Visualization. **Rafeael Romero-Garcia:** Writing - Review & Editing, Supervision. **Michael E. Sughrue:** Conceptualization, Supervision.

## DATA AVAILABILITY STATEMENT

All associated data used in this study is available from publicly sourced databases which are listed in the Acknowledgements. We are able to provide this information upon reasonable request of the corresponding author. The code described in this study is not openly available due to legal restrictions but are available from the corresponding author upon reasonable request. Elements of the code described are private assets of Omniscient Neurotechnology under intellectual property restrictions (patent ID: AU2019903932A0).

## ORCID

Lewis Crawford  <https://orcid.org/0000-0003-2231-5196>

Isabella M. Young  <https://orcid.org/0000-0001-7639-6679>

Rafeael Romero-Garcia  <https://orcid.org/0000-0002-5199-4573>

Michael E. Sughrue  <https://orcid.org/0000-0001-5407-2585>

## REFERENCES

- Auriat, A. M., Borich, M. R., Snow, N. J., Wadden, K. P., & Boyd, L. A. (2015). Comparing a diffusion tensor and non-tensor approach to white matter fiber tractography in chronic stroke. *Neuroimage: Clinical*, 7, 771–781.
- Becker, D., Scherer, M., Neher, P., Jungk, C., Jesser, J., Pflüger, I., ... Unterberg, A. (2020). Going beyond diffusion tensor imaging tractography in eloquent glioma surgery-high-resolution fiber tractography: Q-ball or constrained spherical deconvolution? *World Neurosurgery*, 134, e596–e609.
- Bijsterbosch, J., Harrison, S. J., Jbabdi, S., Woolrich, M., Beckmann, C., Smith, S., & Duff, E. P. (2020). Challenges and future directions for representations of functional brain organization. *Nature Neuroscience*, 23, 1484–1495.
- Bonney, P. A., Conner, A. K., Boettcher, L. B., Cheema, A. A., Glenn, C. A., Smitherman, A. D., ... Sughrue, M. E. (2017). A simplified method of accurate Postprocessing of diffusion tensor imaging for use in brain tumor resection. *Operative Neurosurgery*, 13, 47–59.
- Brett, M., Leff, A. P., Rorden, C., & Ashburner, J. (2001). Spatial normalization of brain images with focal lesions using cost function masking. *Neuroimage*, 14(2), 486–500.
- Briggs, R. G., Allan, P. G., Poologaindran, A., Dadario, N. B., Young, I. M., Ahsan, S. A., ... Sughrue, M. E. (2021). The frontal aslant tract and supplementary motor area syndrome: Moving towards a connectomic initiation axis. *Cancers (Basel)*, 13(5), 1116. <https://doi.org/10.3390/cancers13051116>.
- Briggs, R. G., Conner, A. K., Sali, G., Rahimi, M., Baker, C. M., Burks, J. D., ... Sughrue, M. E. (2018a). A connectomic atlas of the human cerebrum—chapter 16: Tractographic description of the vertical occipital fasciculus. *Operative Neurosurgery*, 15, S456–S461.
- Briggs, R. G., Conner, A. K., Sali, G., Rahimi, M., Baker, C. M., Burks, J. D., ... Sughrue, M. E. (2018b). A connectomic atlas of the human cerebrum—chapter 17: Tractographic description of the cingulum. *Operative Neurosurgery*, 15, S462–S469.
- Briggs, R. G., Rahimi, M., Conner, A. K., Sali, G., Baker, C. M., Burks, J. D., ... Sughrue, M. E. (2018). A connectomic atlas of the human cerebrum—chapter 15: Tractographic description of the uncinate fasciculus. *Operative Neurosurgery*, 15, S450–S455.
- Brodmann, K. (2005). In L. J. Carey (Ed.), *Brodmann's: Localisation in the cerebral cortex*. Berlin: Springer.
- Burks, J. D., Bonney, P. A., Conner, A. K., Glenn, C. A., Briggs, R. G., Battiste, J. D., ... Sughrue, M. E. (2017). A method for safely resecting anterior butterfly gliomas: The surgical anatomy of the default mode network and the relevance of its preservation. *Journal of Neurosurgery*, 126, 1795–1811.
- Calamuneri, A., Arrigo, A., Mormina, E., Milardi, D., Cacciola, A., Chillemi, G., ... Quartarone, A. (2018). White matter tissue quantification at low b-values within constrained spherical deconvolution framework. *Frontiers in Neurology*, 9, 716. <https://doi.org/10.3389/fneur.2018.00716>
- Chen, T., & Guestrin, C. (2016). *XGBoost: A scalable tree boosting method*. New York: Association for Computing Machinery. <https://doi.org/10.1145/2939672.2939785>
- Cheng, H., Wang, Y., Sheng, J., Sporns, O., Kronenberger, W. G., Mathews, V. P., ... Saykin, A. J. (2012). Optimization of seed density in DTI tractography for structural networks. *Journal of Neuroscience Methods*, 203, 264–272.
- Dell'acqua, F., & Tournier, J. D. (2019). Modelling white matter with spherical deconvolution: How and why? *NMR in Biomedicine*, 32, e3945.
- Desikan, R. S., Ségonne, F., Fischl, B., Quinn, B. T., Dickerson, B. C., Blacker, D., ... Killiany, R. J. (2006). An automated labeling system for subdividing the human cerebral cortex on MRI scans into gyral based regions of interest. *NeuroImage*, 31, 968–980.
- Fan, L., Li, H., Zhuo, J., Zhang, Y., Wang, J., Chen, L., ... Jiang, T. (2016). The human brainnetome atlas: A new brain atlas based on connectional architecture. *Cerebral Cortex*, 26, 3508–3526.
- Fischl, B. (2012). FreeSurfer. *Neuroimage*, 62, 774–781.
- Garyfallidis, E., Brett, M., Amirbekian, B., Rokem, A., Van Der Walt, S., Descoteaux, M., ... Dipy Contributors. (2014). Dipy, a library for the analysis of diffusion MRI data. *Frontiers in Neuroinformatics*, 8, 8. <https://doi.org/10.3389/fninf.2014.00008>
- Garyfallidis, E., Brett, M., Correia, M. M., Williams, G. B., & Nimmo-Smith, I. (2012). QuickBundles, a method for tractography simplification. *Frontiers in Neuroscience*, 6, 175–175.
- Glasser, M. F., Coalson, T. S., Robinson, E. C., Hacker, C. D., Harwell, J., Yacoub, E., ... Van Essen, D. C. (2016). A multi-modal parcellation of human cerebral cortex. *Nature*, 536, 171–178.
- Glenn, C., Conner, A. K., Rahimi, M., Briggs, R. G., Baker, C., & Sughrue, M. (2017). Common disconnections in glioma surgery: An anatomic description. *Cureus*, 9, e1778.

- Henschel, L., Conjeti, S., Estrada, S., Diers, K., Fischl, B., & Reuter, M. (2020). FastSurfer: A fast and accurate deep learning based neuroimaging pipeline. *NeuroImage*, 219, 117012.
- Honnorat, N., Parker, D., Tunç, B., Davatzikos, C., & Verma, R. (2017). Subject-specific structural parcellations based on randomized AB-divergences. *Medical Image Computing and Computer-Assisted Intervention*, 10433, 407–415.
- Ille, S., Engel, L., Albers, L., Schroeder, A., Kelm, A., Meyer, B., & Krieg, S. M. (2019). Functional reorganization of cortical language function in glioma patients—A preliminary study. *Frontiers in Oncology*, 9, 446. <https://doi.org/10.3389/FONC.2019.00446/BIBTEX>
- Isensee, F., Schell, M., Pflueger, I., Brugnara, G., Bonekamp, D., Neuberger, U., ... Kickingereder, P. (2019). Automated brain extraction of multisequence MRI using artificial neural networks. *Human Brain Mapping*, 40, 4952–4964.
- Jin, F., Zheng, P., Liu, H., Guo, H., & Sun, Z. (2018). Functional and anatomical connectivity-based parcellation of human cingulate cortex. *Brain and Behavior: A Cognitive Neuroscience Perspective*, 8, e01070.
- Leemans, A., & Jones, D. K. (2009). The B-matrix must be rotated when correcting for subject motion in DTI data. *Magnetic Resonance in Medicine*, 6, 1336–1349. <https://doi.org/10.1002/mrm.21890>
- Li, H., Fan, L., Zhuo, J., Wang, J., Zhang, Y., Yang, Z., & Jiang, T. (2017). ATPP: A pipeline for automatic tractography-based brain parcellation. *Frontiers in Neuroinformatics*, 11, 35. <https://doi.org/10.3389/FNINF.2017.00035/BIBTEX>
- McIntosh, A. R. (2004). Contexts and catalysts: A resolution of the localization and integration of function in the brain. *Neuroinformatics*, 2, 175–182.
- Panesar, S. S., Abhinav, K., Yeh, F.-C., Jacquesson, T., Collins, M., & Fernandez-Miranda, J. (2019). Tractography for surgical neuro-oncology planning: Towards a gold standard. *Neurotherapeutics*, 16, 36–51.
- Pessoa, L. (2014). Understanding brain networks and brain organization. *Physics of Life Reviews*, 11, 400–435.
- Poologaindran, A., Lowe, S. R., & Sughrue, M. E. (2020). The cortical organization of language: Distilling human connectome insights for supratentorial neurosurgery. *Journal of Neurosurgery*, 134, 1959–1966. <https://doi.org/10.3171/2020.5.JNS191281>
- Radwan, A. M., Emsell, L., Blommaert, J., Zhylka, A., Kovacs, S., Theys, T., ... Sunaert, S. (2021). Virtual brain grafting: Enabling whole brain parcellation in the presence of large lesions. *NeuroImage*, 229, 117731. <https://doi.org/10.1016/j.neuroimage.2021.117731>
- Rijnen, S. J. M., Kaya, G., Gehring, K., Verheul, J. B., Wallis, O. C., Sitskoorn, M. M., & Rutten, G. M. (2019). Cognitive functioning in patients with low-grade glioma: Effects of hemispheric tumor location and surgical procedure. *Journal of Neurosurgery*, 133, 1671–1682. <https://doi.org/10.3171/2019.8.JNS191667>
- Romero-Garcia, R., Erez, Y., Oliver, G., Owen, M., Merali, S., Poologaindran, A., ... Hart, M. G. (2020). Practical application of networks in neurosurgery: Combined 3-dimensional printing, neuronavigation, and preoperative surgical planning. *World Neurosurgery*, 137, e126–e137.
- Sali, G., Briggs, R. G., Conner, A. K., Rahimi, M., Baker, C. M., Burks, J. D., ... Sughrue, M. E. (2018). A Connectomic atlas of the human cerebrum—chapter 11: Tractographic description of the inferior longitudinal fasciculus. *Operative Neurosurgery*, 15, S423–S428.
- Smitha, K. A., Akhil Raja, K., Arun, K. M., Rajesh, P. G., Thomas, B., Kapilamoorthy, T. R., & Kesavadas, C. (2017). Resting state fMRI: A review on methods in resting state connectivity analysis and resting state networks. *The Neurology Journal*, 30, 305–317.
- Toselli, B., Tortora, D., Severino, M., Arnulfo, G., Canessa, A., Morana, G., ... Fato, M. M. (2017). Improvement in white matter tract reconstruction with constrained spherical deconvolution and track density mapping in low angular resolution data: A pediatric study and literature review. *Frontiers in Pediatrics*, 5, 182.
- Tournier, J. D., Calamante, F., Gadian, D. G., & Connelly, A. (2004). Direct estimation of the fiber orientation density function from diffusion-weighted MRI data using spherical deconvolution. *NeuroImage*, 23, 1176–1185.
- von Economo, C. F., & Koskinas, G. N. (1925). *Die cytoarchitektonik der hirnrinde des erwachsenen menschen*. J. Springer.
- Wang, Q., Chen, R., Jaja, J., Jin, Y., Hong, L. E., & Herskovits, E. H. (2016). Connectivity-based brain parcellation: A connectivity-based atlas for schizophrenia research. *Neuroinformatics*, 14, 83–97.
- Yeo, B. T. T., Krienen, F. M., Sepulcre, J., Sabuncu, M. R., Lashkari, D., Hollinshead, M., ... Buckner, R. L. (2011). The organization of the human cerebral cortex estimated by intrinsic functional connectivity. *Journal of Neurophysiology*, 106, 1125–1165. <https://doi.org/10.1152/JN.00338.2011>

**How to cite this article:** Doyen, S., Nicholas, P., Poologaindran, A., Crawford, L., Young, I. M., Romero-Garcia, R., & Sughrue, M. E. (2022). Connectivity-based parcellation of normal and anatomically distorted human cerebral cortex. *Human Brain Mapping*, 43(4), 1358–1369. <https://doi.org/10.1002/hbm.25728>